

The Mg II $\lambda 2797$, $\lambda 2803$ emission in low-metallicity star-forming galaxies from the SDSS*

N. G. Guseva^{1,2}, Y. I. Izotov^{1,2}, K. J. Fricke^{1,3}, and C. Henkel^{1,4}

¹ Max-Planck-Institut für Radioastronomie, Auf dem Hügel 69, 53121 Bonn, Germany

² Main Astronomical Observatory, Ukrainian National Academy of Sciences, Zabolotnoho 27, Kyiv 03680, Ukraine

³ Institut für Astrophysik, Göttingen Universität, Friedrich-Hund-Platz 1, 37077 Göttingen, Germany

⁴ Astronomy Department, King Abdulaziz University, P.O. Box 80203, Jeddah, Saudi Arabia

Received

; Accepted

ABSTRACT

We present 65 Sloan Digital Sky Survey (SDSS) spectra of 62 star-forming galaxies with oxygen abundances $12 + \log O/H \sim 7.5 - 8.4$. Redshifts of selected galaxies are in the range $z \sim 0.36 - 0.70$. This allows us to detect the redshifted Mg II $\lambda 2797$, $\lambda 2803$ emission lines. Our aim is to use these lines for the magnesium abundance determination. The Mg II emission was detected in $\sim 2/3$ of the galaxies. We find that the Mg II $\lambda 2797$ emission-line intensity follows a trend with the excitation parameter $x = O^{2+}/O$ that is similar to that predicted by CLOUDY photoionised H II region models, suggesting a nebular origin of Mg II emission. The Mg/O abundance ratio is lower by a factor ~ 2 than the solar ratio. This is probably the combined effect of interstellar Mg II absorption and depletion of Mg onto dust. However, the effect of dust depletion in selected galaxies, if present, is small, by a factor of ~ 2 lower than that of iron.

Key words. galaxies: abundances — galaxies: irregular — galaxies: evolution — galaxies: formation — galaxies: ISM — H II regions — ISM: abundances

1. Introduction

Magnesium is an α -process element produced during nuclear burning in massive stars, which is similar to oxygen and some other elements, such as noble neon and argon. Its abundance is studied in detail from absorption lines in stars with a wide range of metallicities and shows trends similar to oxygen.

The Mg II $\lambda\lambda 2797, 2803\text{\AA}$ doublet (h and k) is one of the most studied tracers of the gas-phase medium in planetary nebulae (PNe), in the Local InterStellar Medium (LISM) of the Galaxy, and in the gaseous environment of distant galaxies. Since magnesium, which is similar to silicon and iron among other elements, is a refractory element, its abundance can provide information about the level of interstellar magnesium depletion onto dust.

The magnesium abundance in the LISM can be determined by analysing absorption lines towards Galactic stars. With high-resolution spectra of many Galactic early-type stars observed from *Copernicus* launched in 1972 it was found that profiles of Mg II h and k lines are identical with solar profiles except for the presence of narrow absorption components formed in the interstellar medium along the line of sight (Oegerle et al. 1982; Murray 1983). Follow-up observations of early type and cool stars with the *IUE* (*International Ultraviolet Explorer*) and the *HST* (*Hubble Space Telescope*) provided quantitative characteristics of the interstellar medium towards Galactic stars and planetary nebulae: the distribution of the magnesium abundance in the LISM (Molaro et al. 1986; Middlemass 1988), specifically; the structure of the LISM within 100 pc (Redfield & Linsky 2004); and the abundances and physical conditions in the dif-

fuse interstellar clouds (Welty et al. 1999). These data indicate a moderate level of magnesium depletion.

There are only a few determinations of the magnesium abundance in H II regions, such as the Orion nebula in the Galaxy and the Tarantula nebula in the Large Magellanic Cloud and in some bright planetary nebulae (Rodríguez & Rubin 2005; Peimbert & Peimbert 2010; Dinerstein et al. 2012). Dinerstein et al. (2012) has investigated the gas-phase magnesium abundances in 25 planetary nebulae using the Mg II $\lambda 4481\text{\AA}$ recombination line. They find that Mg/H is close to solar, implying that Mg is at most minimally depleted, whereas the measurements in the 30 Doradus and the Orion nebulae, with the same recombination line, indicate significantly higher levels of Mg depletion up to 72% and 90%, respectively (Peimbert & Peimbert 2010).

The Mg II $\lambda\lambda 2707, 2803\text{\AA}$ doublet is the strongest absorption feature that is detectable in the optical range at intermediate redshifts ($0.3 \leq z \leq 2$). Therefore, magnesium absorption lines are often detected in spectra of background quasars and galaxies. Spectra of background sources allow us to probe regions of low-ionisation and cool gas present in the outer regions of spiral discs and dwarf irregular galaxies (Dessauges-Zavadsky et al. 2004). Many Mg II surveys have been carried out for these systems (Sargent et al. 1988; Steidel & Sargent 1992; Dessauges-Zavadsky et al. 2003; York et al. 2006; Prochter et al. 2006; Prochaska et al. 2007; Lilly et al. 2007; Quider et al. 2011). Owing to large spectroscopic surveys including the Sloan Digital Sky Survey (SDSS) (York et al. 2000) hundreds of thousands of quasars have been used to identify large samples of absorption systems along the line of sight using the Mg II absorption lines (York et al. 2006; Bouché et al. 2006; Prochter et al. 2006; Lundgren et al.

Send offprint requests to: N. G. Guseva, guseva@mao.kiev.ua

* Table 2 is only available in the electronic edition.

2009; Quider et al. 2011). Recently, based on a fully-automatic method, Zhu & Ménard (2012) compiled a very large sample of $\sim 40,000$ Mg II absorbers from the SDSS Data Release 7 (DR7).

Using the Mg II absorber samples many detailed studies on the distribution of column densities, the redshift evolution of densities, and the kinematic signatures e.g., (outflowing material from star-forming regions) have been performed (Steidel & Sargent 1992; Nestor et al. 2005; Prochter et al. 2006). Based on 4000 Mg II absorbers from zCOSMOS (Lilly et al. 2007), Bordoloi et al. (2011) find that at the same stellar mass, the strength of Mg II absorption is much higher for blue star-forming galaxies than for red galaxies. Determinations of the Mg abundances from the absorption lines in damped Ly α absorbing (DLA) systems gave Mg/O abundance ratios that are close to the solar values. Meanwhile, the absorption line systems allow investigations of gas properties in outer parts of galaxies and in the intergalactic medium.

Element abundances of the interstellar medium are usually compared with the solar abundances, assuming that the interstellar medium has the same composition as the Sun, which is, however, not the case (Snow & Witt 1996). Instead, the depletion will be different if the reference standard is derived from different types of stars in the solar neighbourhood, or the solar neighbourhood abundances corrected for the chemical evolution of the Galaxy, since formation of the Sun, or taking the galactocentric gradient of the chemical elements into account (Snow & Witt 1996; Peimbert & Peimbert 2010). Thus, Snow & Witt (1996) found systematically lower depletions using different so-called ‘‘cosmic’’ abundances as reference. Different authors also use different solar abundances as reference abundance (e.g. Grevesse & Sauval 1998; Asplund et al. 2005, 2009) or solar system meteoritic values, and different metallicity indicators (O, S, Zn) in DLA, QSO, and GRB absorption systems. Using such different reference abundances resulted in a Mg depletion that does not exceed ~ 0.2 dex. (Throughout the paper we use solar values by Asplund et al. 2009).

However, despite numerous magnesium abundance determinations, only upper limits of Mg II abundances have been obtained in the overwhelming majority of the cases. There is also a problem with some O I absorption oxygen lines since those are generally saturated. Therefore there are not so many exact Mg/O abundance ratios derived in DLAs.

No such determinations exist for extragalactic H II regions, excluding the Tarantula nebula. This is because of the weakness of the Mg II $\lambda 4481\text{\AA}$ recombination line seen in emission, and its blending with other weak emission lines. The only possibility for studying the Mg abundance in extragalactic H II regions is to use intensities of the resonance doublet Mg II $\lambda 2797$, $\lambda 2803$ lines, which are much brighter than the recombination lines. However, these emission lines, at variance to forbidden lines, are subject to absorption by the weakly ionised interstellar medium. It is also possible that in some galaxies gas outflows can be responsible for an additional underlying contribution to the Mg II lines producing broad features due to the Doppler effect. However, for our galaxy sample we cannot consider the effects of Mg gas outflows and radiation transfer in the medium surrounding the H II regions due to the unknown gas velocity distribution and ionisation structure of our objects. Additionally, Mg II $\lambda 2797$, $\lambda 2803$ emission and absorption can be produced by cool giant and supergiant stars, and luminous blue variable (LBV) stars.

Finally, the doublet in spectra of low-redshift galaxies can only be observed from space. However, in higher redshift galaxies, Mg II $\lambda 2797$, $\lambda 2803$ lines can be measured in the optical range. In particular, these lines are seen in the SDSS spectra with

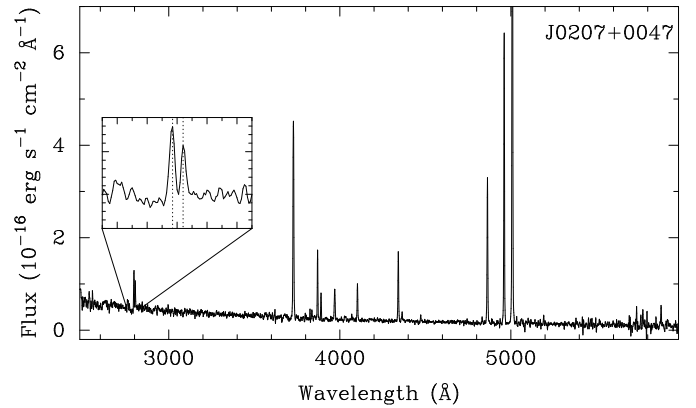


Fig. 1. The redshift-corrected SDSS spectrum of J0207+0047. The spectral region $\lambda\lambda 2750 - 2850$, which includes the Mg II $\lambda 2797$, $\lambda 2803$ emission lines, is shown in the inset. Vertical dotted lines in the inset indicate the nominal wavelengths of the lines.

a lower wavelength cut-off of $\sim 3800\text{\AA}$ if the galaxy redshift z is greater than ~ 0.36 , allowing the determination of its abundance.

The aim of this paper is to select SDSS spectra of emission-line star-forming galaxies with $z \gtrsim 0.36$ showing the Mg II $\lambda 2797$, $\lambda 2803$ doublet in emission and to derive Mg abundances. Our sample of emission-line galaxies extracted from the SDSS is discussed in Section 2. The element abundances are derived in Section 3. We discuss our results and compare them with other types of objects in Section 4. Our main findings are summarised in Section 5.

2. Sample of SDSS galaxies

We use a sample that is composed of spectra of low-metallicity H II regions with strong emission lines selected from the SDSS DR7. The SDSS (York et al. 2000) offers a gigantic data base of galaxies with well-defined selection criteria that are observed in a homogeneous way. First, we extracted ~ 15000 spectra with strong emission lines from the whole data base of ~ 800000 galaxy spectra. Out of this sample we selected 65 spectra of star-forming galaxies with strong nebular H β , H α , [O II] $\lambda 3727$, [O III] $\lambda 4959$, $\lambda 5007$ emission lines and redshifts $z \gtrsim 0.36$. The [O III] $\lambda 4363$ emission line is also present in many of these spectra (in $\sim 63\%$ of the total sample and $\sim 70\%$ of the galaxies in which Mg II lines were detected), allowing an accurate determination of the oxygen abundance by the direct T_e -method. For three galaxies, two spectra are available in the SDSS data base. Therefore, the total number of selected galaxies is 62.

The general characteristics of the selected galaxies are shown in Table 1. The redshift range is 0.36 – 0.70. In general these galaxies are very faint, with the apparent SDSS g magnitude fainter than 19 mag. The redshift-corrected spectrum of one galaxy, J0207+0047, is shown in Fig. 1. This spectrum resembles the spectrum of high-excitation star-forming H II region with strong emission lines, including [O III] $\lambda 4363$. The Mg II $\lambda 2797$, $\lambda 2803$ doublet is also present in emission and it is shown in more detail in the inset. The remaining 64 redshift-corrected spectra in the wavelength range $\lambda\lambda 2750 - 2850\text{\AA}$ are shown in Fig. 2. Despite the noisy spectra in some cases, the Mg II emission is detected in about two thirds of the spectra. However, we also note that blue-shifted Mg II absorption is present in many cases, which may be an indication of stellar winds from cool massive stars, such as LBVs. In some cases broad absorption features are

Table 1. General characteristics of galaxies

Name	R.A.(J2000)	Dec.(J2000)	z	g^a	Name	R.A.(J2000)	Dec.(J2000)	z	g^a
J0006-0903	00:06:14.94	-09:03:16.59	0.4296	19.61	J0925+2709	09:25:49.14	+27:09:28.45	0.4891	20.03
J0101-0057	01:01:05.92	-00:57:29.65	0.3903	20.39	J0956+3203	09:56:21.73	+32:03:54.89	0.4263	20.62
J0104+0013	01:04:45.44	+00:13:25.28	0.4909	20.38	J0957+3314	09:57:24.75	+33:14:08.14	0.5300	21.17
J0142+0108	01:42:57.53	+01:08:24.47	0.5242	19.79	J1000+3324	10:00:59.49	+33:24:17.95	0.3890	21.61
J0149+0100	01:49:47.60	+01:00:09.70	0.5660	20.65	J1002+3228	10:02:21.48	+32:28:26.38	0.4854	21.66
J0155-0107	01:55:28.88	-01:07:47.01	0.4146	20.64	J1007+0446	10:07:58.98	+04:46:26.24	0.4167	20.44
J0207+0047	02:07:48.00	+00:47:35.43	0.5400	19.98	J1045+3225	10:45:29.29	+32:25:32.13	0.4094	19.42
J0232-0021	02:32:41.75	-00:21:23.53	0.3678	19.82	J1048+6359	10:48:39.03	+63:59:21.55	0.3738	20.21
J0301-0806	03:01:39.58	-08:06:45.20	0.4314	21.84	J1056+4758	10:56:42.43	+47:58:50.81	0.4347	21.45
J0319-0104	03:19:59.81	-01:04:49.98	0.6295	20.30	J1108+6344	11:08:54.82	+63:44:05.59	0.4395	20.51
J0340-0048	03:40:47.92	-00:48:48.12	0.4503	22.11	J1112+6331	11:12:19.22	+63:31:48.85	0.4115	21.08
J0747+3147	07:47:54.23	+31:47:16.59	0.3781	21.59	J1128-0317	11:28:47.68	-03:17:17.48	0.5563	20.34
J0749+3142	07:49:48.00	+31:42:49.11	0.6959	21.11	J1135+6025	11:35:27.96	+60:25:32.99	0.4299	19.13
J0756+3057	07:56:43.78	+30:57:29.49	0.4213	21.68	J1136-0223	11:36:27.54	-02:23:17.80	0.3931	20.92
J0757+3148	07:57:27.88	+31:48:59.87	0.6148	21.43	J1213+2705	12:13:09.77	+27:05:38.58	0.3830	19.35
J0804+1748	08:04:23.50	+17:48:25.17	0.5498	21.27	J1408+0224	14:08:06.07	+02:24:09.19	0.4041	20.22
J0807+4002	08:07:59.23	+40:02:18.74	0.4712	21.15	J1420+2628	14:20:01.22	+26:28:04.29	0.3872	19.34
J0812+3200	08:12:41.86	+32:00:46.38	0.4562	21.46	J1430+4802	14:30:55.90	+48:02:01.58	0.4775	20.70
J0813+3339	08:13:36.62	+30:39:35.60	0.5584	20.93	J1544+3308	15:44:18.78	+33:08:47.84	0.4000	19.80
J0815+3129	08:15:24.40	+31:29:36.05	0.4055	20.83	J1548+0727	15:48:14.67	+07:27:10.13	0.4170	20.20
J0817+3159	08:17:06.28	+31:59:00.75	0.4083	20.79	J1555+3543	15:55:16.39	+35:43:24.65	0.4519	19.79
J0837+3108	08:37:57.41	+31:08:40.39	0.5144	21.00	J1559+0634	15:59:08.55	+06:34:38.86	0.5369	20.00
J0838+3057	08:38:57.85	+30:57:50.22	0.5552	21.74	J1602+4002	16:02:06.36	+40:02:49.11	0.3885	00.00
J0844+3241	08:44:31.93	+32:41:05.99	0.5988	21.75	J1616+2057	16:16:42.64	+20:57:20.11	0.5988	20.30
J0855+0318	08:55:58.30	+03:18:07.47	0.4359	21.66	J1716+2744	17:16:00.88	+27:44:14.40	0.4867	19.50
J0904+2806	09:04:46.04	+28:06:05.65	0.3859	19.66	J2145+0040	21:45:51.41	+00:40:30.93	0.4179	20.38
J0914+4451	09:14:57.59	+44:51:10.46	0.4430	21.12	J2208-0106	22:08:40.38	-01:06:12.29	0.5115	20.78
J0915+3344	09:15:23.10	+33:44:29.77	0.3948	21.51	J2211+0114	22:11:45.46	+01:14:08.44	0.3721	20.35
J0918+3301	09:18:10.90	+33:01:42.09	0.5112	21.50	J2334-0046	23:34:36.23	-00:46:36.61	0.5245	20.34
J0918+3331	09:18:28.35	+33:31:06.56	0.6334	21.37	J2348-0041	23:48:09.07	-00:41:01.66	0.4095	20.22
J0922+3330	09:22:38.44	+33:30:13.29	0.4267	21.82	J2352+0025	23:52:37.96	+00:25:58.77	0.6354	20.17

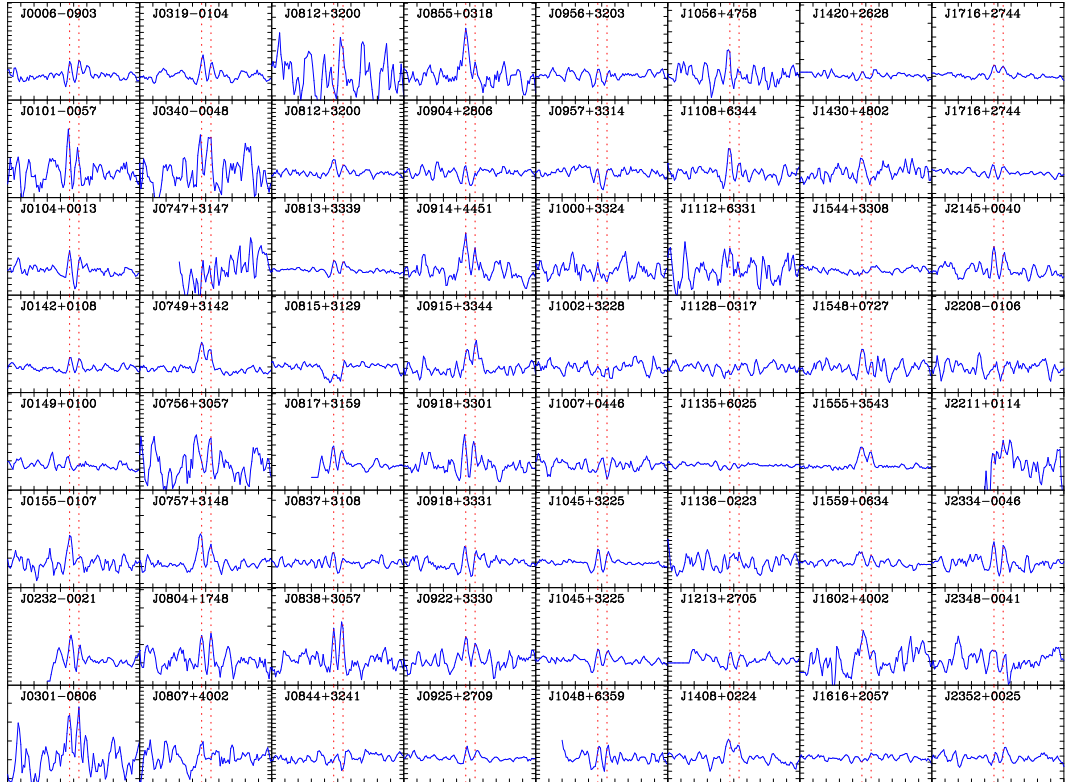
^a Apparent SDSS g magnitude.

Fig. 2. The redshift-corrected SDSS spectra in the wavelength range $\lambda\lambda 2750 - 2850\text{\AA}$ of all selected galaxies excluding J0207+0047, which is shown in Fig. 1. Vertical dotted lines indicate the nominal wavelengths of the Mg II $\lambda 2797$, $\lambda 2803$ emission lines. For three galaxies, J0812+3200, J1045+3225, and J1716+2744, two spectra are shown that available in the SDSS data base.

Table 3. Input parameters for the grid of the photoionised H II region models

Parameter	Value
$\log Q(\text{H})^a$	52, 53, 54
Starburst age, Myr	2.0, 3.5, 4.0
N_e^b	10, 10^2 , 10^3 , var
$\log f^c$	-0.5, -1.0, -1.5, -2.0
Oxygen abundance $12+\log\text{O}/\text{H}$	7.3, 7.6, 8.0, 8.3
^4He mass fraction Y	0.254

^alog of the number of ionising photons in units s^{-1} .

^bThe electron number density in units cm^{-3} . The electron number density in models labelled “var” is varied with radial distance according to Eq. 1.

^clog of volume filling factor.

Table 4. Coefficients for the $ICF(\text{Mg}^+)^a$ fit in Eq. 5

i	a_i	b_i	c_i
1	4.4102×10^{-21}	2.2063×10^2	5.3269×10^4
2	9.2000×10^{-9}	2.5726×10^1	2.3156×10^1
3	9.2671×10^{-4}	-2.2616×10^0	1.0263×10^1
4	1.3081×10^0	-2.7979×10^{-1}	1.3332×10^0

^a ICF is the ionisation correction factor.

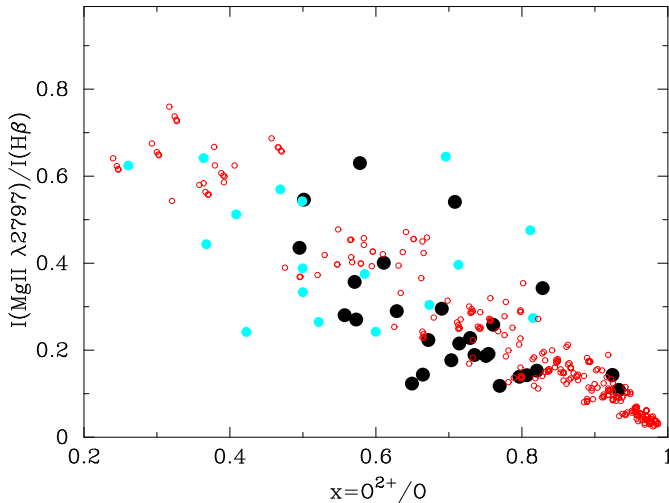


Fig. 3. Dependence of $I(\text{Mg II } \lambda 2797)/I(\text{H}\beta)$ on the excitation parameter $x = \text{O}^{2+}/\text{O}$. Red open circles are data from CLOUDY models calculated by adopting $12 + \log\text{O}/\text{H} = 8.0$ and 8.3 . Large black filled circles are extinction-corrected intensities for the H II regions with $12 + \log\text{O}/\text{H} \geq 7.9$ and small light blue filled circles with $12 + \log\text{O}/\text{H} < 7.9$.

observed at the position of Mg II $\lambda 2797\text{\AA}$ and $\lambda 2803\text{\AA}$ emission lines. The most prominent feature of this kind is seen in the spectrum of J0815+3129. In some other cases absorption features are absent in the spectra. We take all these peculiarities into account and measure the emission line intensities by placing a continuum level at the bottom of the absorption profiles if they are present.

The extinction-corrected line fluxes $I(\lambda)$, normalised to $I(\text{H}\beta)$, are given in Table 2. They are only available in the electronic online version. The line fluxes were obtained using the IRAF¹ SPLIT routine. The line flux errors include statistical

¹ IRAF is the Image Reduction and Analysis Facility distributed by the National Optical Astronomy Observatory, which is operated by the Association of Universities for Research in Astronomy (AURA) under cooperative agreement with the National Science Foundation (NSF).

errors in addition to errors introduced by the standard star absolute flux calibration, which we set to 1% of the line fluxes. These errors will be propagated later into the calculation of abundance errors. The line fluxes were corrected for two effects: (1) reddening using the extinction curve of Cardelli et al. (1989) and (2) underlying hydrogen stellar absorption derived simultaneously by an iterative procedure as described in Izotov et al. (1994). Since the redshifts of the selected galaxies are high, the correction for extinction was done in two steps. First, emission-line intensities with observed wavelengths were corrected for the Milky Way extinction, using values of the extinction $A(V)$ in the V band from the NASA/IPAC extragalactic database (NED). Then, the internal extinction was derived from the Balmer hydrogen emission lines, corrected for the Milky Way extinction. The internal extinction was applied to correct line intensities at non-redshifted wavelengths. The extinction coefficients in both cases of the Milky Way and the internal extinction are defined as $C(\text{H}\beta) = 1.47E(B - V)$, where $E(B - V) = A(V)/3.2$ (Aller 1984). The mean value of the internal extinction coefficient $C(\text{H}\beta) \sim 0.2$ is typical of star-forming galaxies.

Additionally, the Mg II $\lambda 2797$, $\lambda 2803$ emission lines were corrected for the underlying stellar absorption. For this, we used the Bruzual & Charlot (2003) population synthesis models of single stellar populations. Spectra of these models do not have sufficient spectral resolution to separate Mg II $\lambda 2797$ and $\lambda 2803$ absorption lines. Therefore, we measured the equivalent width of the blend. We find that in a wide range of starburst ages of 3 – 10 Myr, the equivalent width $\text{EW}_{\text{abs}}(\text{Mg II } \lambda 2797 + \lambda 2803)$ is constant and is equal to $\sim -1\text{\AA}$. The “-” sign means that the line is in absorption. Then, for separate Mg II absorption lines we adopt equal EW_{abs} ’s of -0.5\AA and correct Mg II emission lines multiplying their intensities by a factor $(\text{EW} + |\text{EW}_{\text{abs}}|)/\text{EW}$, where EW is the equivalent width of the emission line. Equivalent widths $\text{EW}(\text{H}\beta)$, extinction coefficients $C(\text{H}\beta)(\text{MW})$ and $C(\text{H}\beta)(\text{int})$, and EW_{abs} of the hydrogen absorption stellar lines are also given in Table 2, along with the uncorrected H β fluxes.

3. Element abundances

3.1. Oxygen abundance

To determine element abundances, we generally follow the procedures of Izotov et al. (1994, 1997) and Thuan et al. (1995). We adopt a two-zone photoionised H II region model: a high-ionisation zone with temperature $T_e(\text{O III})$, where the [O III] lines originate, and a low-ionisation zone with temperature $T_e(\text{O II})$, where the [O II] lines originate. In the H II regions with a detected [O III] $\lambda 4363$ emission line, the temperature $T_e(\text{O III})$ is calculated using the direct method based on the [O III] $\lambda 4363/(\lambda 4959 + \lambda 5007)$ line ratio. In H II regions where the [O III] $\lambda 4363$ emission line is not detected, we used a semi-empirical method described by Izotov & Thuan (2007) to derive $T_e(\text{O III})$. For $T_e(\text{O II})$, we use the relation between the electron temperatures $T_e(\text{O III})$ and $T_e(\text{O II})$ obtained by Izotov et al. (2006) from the H II photoionisation models (Stasińska & Izotov 2003).

Ionic and total oxygen abundances are derived using expressions for ionic abundances obtained by Izotov et al. (2006). For magnesium, we assume that the Mg II emission has a nebular origin (see text below and Fig. 3). Then the magnesium abundance can be derived if the electron temperature $T_e(\text{Mg II})$ in the Mg^+ zone and the ionisation correction factor $ICF(\text{Mg}^+)$ for unseen stages of ionisation are known. To derive $T_e(\text{Mg II})$ and

Table 5. Spectroscopic parameters

Object	12+logO/H	[Mg/O]	EW(H β) ^b	Object	12+logO/H	[Mg/O]	EW(H β) ^b
J0006–0903	7.96±0.05	–0.19±0.15	50	J0956+3203	7.66±0.06	+0.00±0.00	43
J0101–0057	7.96±0.02	–0.03±0.10	64	J0957+3314	7.78±0.02	–0.36±0.10	39
J0104+0013	8.12±0.06	–0.12±0.18	49	J1000+3324	7.82±0.02	+0.00±0.00	48
J0142+0108	8.05±0.04	–0.31±0.14	68	J1002+3228	7.58±0.02	+0.00±0.00	50
J0149+0100	7.96±0.02	...	94	J1007+0446	7.80±0.01	...	65
J0155–0107	8.04±0.02	–0.49±0.11	185	J1045+3225 ^a	8.19±0.03	–0.45±0.10	77
J0207+0047	8.22±0.02	–0.24±0.09	107	J1045+3225 ^a	8.24±0.03	–0.38±0.11	75
J0232–0021	8.20±0.05	–0.58±0.17	82	J1048+6359	7.57±0.01	–0.34±0.06	42
J0301–0806	7.83±0.01	–0.15±0.09	167	J1056+4758	8.00±0.01	–0.24±0.11	431
J0319–0104	8.06±0.02	–0.36±0.08	94	J1108+6344	8.04±0.02	–0.49±0.10	108
J0340–0048	7.89±0.01	–0.24±0.07	199	J1112+6331	7.77±0.01	...	132
J0747+3147	7.84±0.03	...	78	J1128–0317	7.95±0.02	...	32
J0749+3142	7.87±0.02	+0.00±0.09	147	J1135+6025	7.66±0.05	...	38
J0756+3057	7.66±0.02	–0.13±0.07	50	J1136–0223	7.96±0.01	...	38
J0757+3148	8.05±0.02	–0.04±0.09	147	J1213+2705	7.72±0.01	–0.44±0.05	35
J0804+1748	8.06±0.02	–0.38±0.09	165	J1408+0224	7.82±0.01	–0.14±0.08	131
J0807+4002	7.87±0.02	...	120	J1420+2628	8.29±0.06	...	59
J0812+3200 ^a	7.94±0.02	...	339	J1430+4802	7.87±0.01	...	45
J0812+3200 ^a	8.15±0.03	–0.44±0.17	116	J1544+3308	7.62±0.01	...	32
J0813+3339	7.69±0.02	–0.20±0.11	43	J1548+0727	8.19±0.03	–0.39±0.10	126
J0815+3129	7.64±0.02	...	25	J1555+3543	8.31±0.05	–0.32±0.16	95
J0817+3159	8.25±0.04	–0.36±0.15	117	J1559+0634	7.82±0.01	–0.34±0.08	32
J0837+3108	7.86±0.05	–0.58±0.21	63	J1602+4002	7.94±0.01	...	47
J0838+3057	8.07±0.01	–0.53±0.12	113	J1616+2057	8.03±0.04	...	91
J0844+3241	7.83±0.08	–0.15±0.25	62	J1716+2744 ^a	7.88±0.01	–0.34±0.04	44
J0855+0318	7.83±0.01	–0.04±0.06	388	J1716+2744 ^a	7.95±0.01	–0.37±0.04	44
J0904+2806	7.53±0.10	–0.20±0.26	31	J2145+0040	7.84±0.01	–0.25±0.05	66
J0914+4451	7.92±0.01	–0.56±0.07	170	J2208–0106	7.89±0.01	...	71
J0915+3344	8.11±0.09	–0.25±0.29	207	J2211+0114	7.77±0.01	–0.53±0.09	28
J0918+3301	8.44±0.09	–0.02±0.30	424	J2334–0046	7.91±0.01	–0.25±0.05	54
J0918+3331	7.52±0.11	–0.15±0.31	61	J2348–0041	8.05±0.03	...	100
J0922+3330	8.00±0.02	–0.49±0.17	131	J2352+0025	8.18±0.05	–0.41±0.18	64
J0925+2709	8.36±0.08	–0.56±0.28	73				

^aGalaxies with two available spectra in the SDSS.

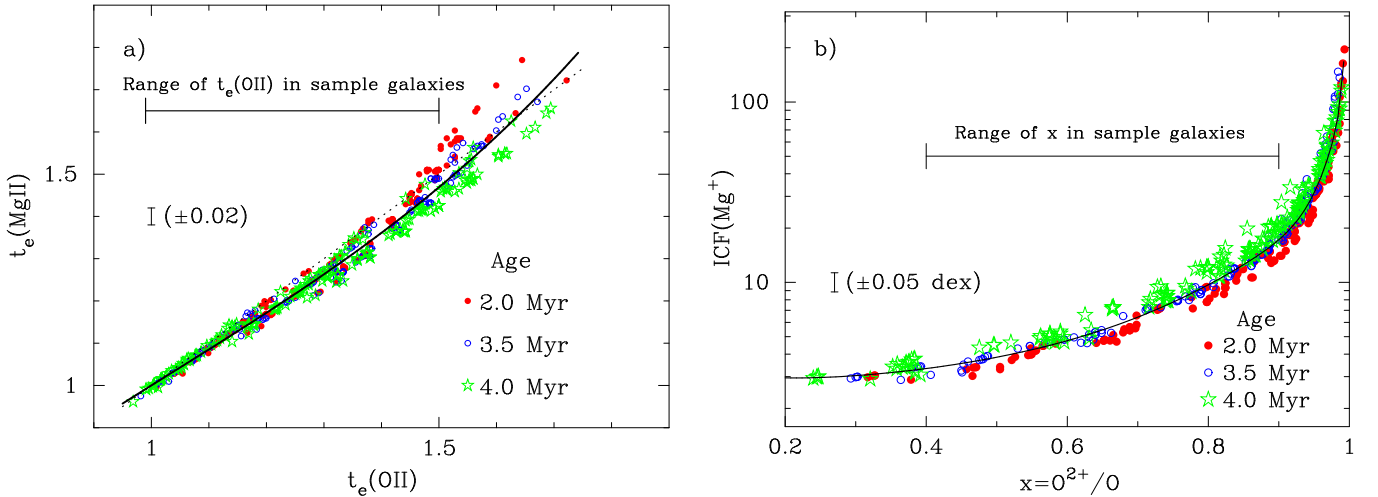
^bin Å.


Fig. 4. (a) The relation between the electron temperatures $t_e(\text{Mg II})$ and $t_e(\text{O II})$. t_e are in units of $10^{-4}T_e$. Red filled circles, blue open circles, and green stars are data from CLOUDY models with starburst ages of 2.0 Myr, 3.5 Myr, and 4.0 Myr, respectively. The solid line is the fit to data with all ages, defined by Eq. 2. The dotted line is the line of equal temperatures. The range of the electron temperature $t_e(\text{O II})$ in the sample galaxies is shown by a horizontal line. The error bar is the dispersion of $t_e(\text{Mg II})$ in the range of $t_e(\text{O II})$ shown by the horizontal line. (b) The relation between the ionisation correction factor $ICF(\text{Mg}^+)$ and the excitation parameter $x = \text{O}^{2+}/\text{O}$. Red filled circles, blue open circles, and green stars are data from CLOUDY models with starburst ages of 2.0 Myr, 3.5 Myr, and 4.0 Myr, respectively. The solid line is the fit to data with all ages as defined by Eq. 5 with the coefficients from Table 3. The range of the excitation parameter x in the sample galaxies is shown by a horizontal line. The error bar is the dispersion of $ICF(\text{Mg}^+)$ (in dex) in the range of x shown by the horizontal line.

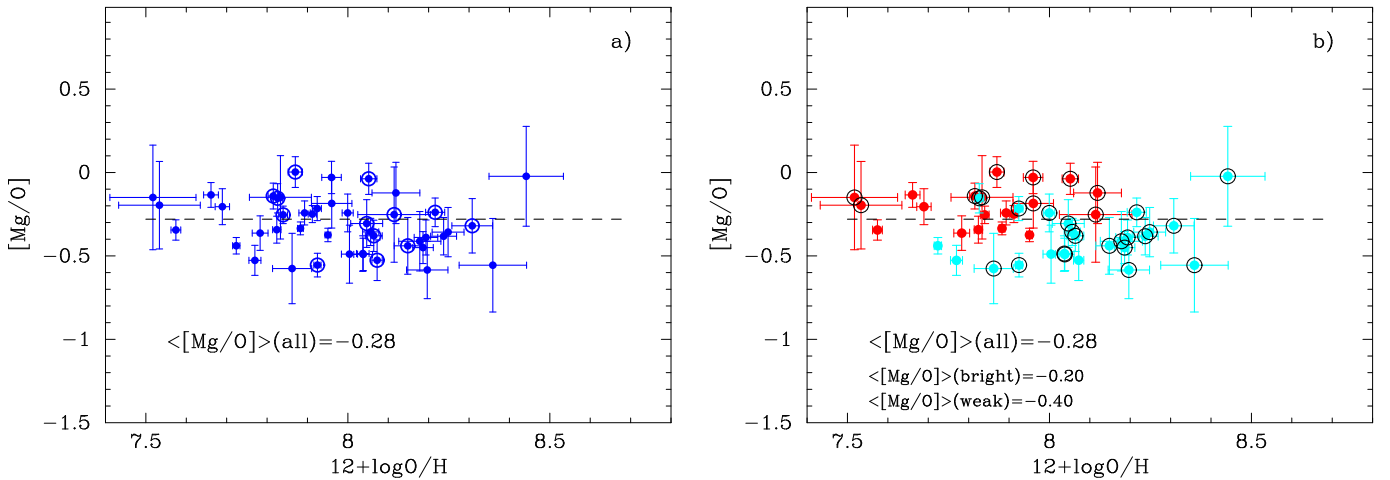


Fig. 5. Dependence of the magnesium-to-oxygen abundance ratio relative to the solar value, $[\text{Mg}/\text{O}] = \log(\text{Mg}/\text{O}) - \log(\text{Mg}/\text{O})_{\odot}$, on oxygen abundance $12+\log\text{O}/\text{H}$ with error bars for all data points. The solar value $\log(\text{Mg}/\text{O})_{\odot} = -1.09$ is adopted from Asplund et al. (2009). Dashed line and $\langle[\text{Mg}/\text{O}]\rangle$ in both panels are mean values of $[\text{Mg}/\text{O}]$. (a) The encircled galaxies are those with no clear presence of blue-shifted absorption profiles (Fig. 2). (b) The same sample as in (a) but with division between bright Mg II lines with $I(\lambda 2797\text{\AA})/I(\text{H}\beta) \geq 0.3$ (red filled circles) and weak Mg II lines with $I(\lambda 2797\text{\AA})/I(\text{H}\beta) < 0.3$ (blue filled circles). Encircled galaxies in (b) are those where $[\text{O III}]\lambda 4363\text{\AA}$ is measured. Additionally, the mean values of $[\text{Mg}/\text{O}]$ for bright ($\langle[\text{Mg}/\text{O}]\rangle(\text{bright})$) and weak ($\langle[\text{Mg}/\text{O}]\rangle(\text{weak})$) Mg II lines are denoted.

$ICF(\text{Mg}^+)$ we use a grid of the photoionised H II region models that also predict Mg II $\lambda 2797$, $\lambda 2803$ emission-line intensities.

3.2. Grid of photoionisation CLOUDY models

Using the version v10.00 of the CLOUDY code (Ferland et al. 1998) we calculated a grid of 432 spherical ionisation-bounded H II region models with parameters shown in Table 3, which cover the entire range of parameters in real high-excitation, low-metallicity H II regions. In particular, the range of oxygen abundances is $12 + \log \text{O}/\text{H} \approx 7.5 - 8.4$ for our sample. The abundances of other heavy elements relative to oxygen are kept constant and correspond to the typical value obtained for low-metallicity emission-line galaxies (e.g. Izotov et al. 2006). We also include dust, scaling it according to the oxygen abundance. The characteristics adopted for the dust are those offered by CLOUDY as ‘‘Orion nebula dust’’.

We adopt three values of the number of ionising photons Q and the shape for the ionising radiation spectrum corresponding to the Starburst99 model with the ages of 2.0, 3.5, and 4.0 Myr and different metallicities (Leitherer et al. 1999). Thus, for $12+\log\text{O}/\text{H} = 7.3$ and 7.6 we adopt Starburst99 models with the heavy element mass fraction $Z = 0.001$, for those with $12+\log\text{O}/\text{H} = 8.0$ models with $Z = 0.004$ and for those with $12+\log\text{O}/\text{H} = 8.3$ models with $Z = 0.008$. All Starburst99 models were calculated with the Hillier & Miller (1998) and Pauldrach et al. (2001) stellar atmosphere set and with the stellar tracks from Meynet et al. (1994). We also vary the log of volume-filling factor f between -0.5 and -2.0 to obtain CLOUDY models with different ionisation parameters.

Our range of the number density, $N_e = 10 - 10^3 \text{ cm}^{-3}$, which is kept constant along a given H II region radius, covers the whole range expected for the extragalactic H II regions. Additionally, we calculated a set of 144 H II region models with parameters from Table 3 (excluding N_e) with a Gaussian density distribution as a function of radius r according to

$$N_e(r) = N_e(0) \exp\left[-\frac{r^2}{(30 \text{ pc})^2}\right], \quad (1)$$

where $N_e(0) = 10^3 \text{ cm}^{-3}$. Thus, the total number of the models, which we use for the subsequent analysis, is 576.

Since the CLOUDY code allows us to predict Mg II line intensities, we compared these intensities with the observed ones. The result of the comparison is shown in Fig. 3 where we show the Mg II $\lambda 2797$ line intensity as a function of the excitation parameter $x = \text{O}^{2+}/\text{O}$. The observed H II regions with $12 + \log\text{O}/\text{H} \geq 7.9$ are shown by large black filled circles and H II regions with $12 + \log\text{O}/\text{H} < 7.9$ by small light blue filled circles. Thus, the range of oxygen abundances in most of our galaxies is $12 + \log\text{O}/\text{H} \sim 7.7 - 8.4$ (see Table 5). Therefore, we show in Fig. 3 only predicted Mg II $\lambda 2797$ line intensities in the models with $12+\log\text{O}/\text{H} = 8.0$ and 8.3 (red open circles). Our comparison shows that in general extinction-corrected Mg II $\lambda 2797$ observed intensities are by a factor of ~ 1.3 lower than the predicted ones even for the H II regions with $12 + \log\text{O}/\text{H}$ between 7.9 and 8.4 , but they follow a trend with x which is similar to the trend for predicted intensities. This implies that Mg II $\lambda 2797$ emission is most likely nebular in origin, and the reduced line intensities are due to the combined effect of interstellar absorption and Mg depletion onto dust.

3.3. Magnesium abundance

The electron temperature $T_e(\text{Mg II})$ in the Mg^+ zone and $T_e(\text{O II})$ in the O^+ zone are obtained from the CLOUDY photoionised H II region models. In Fig. 4a we show the relation between the electron temperatures in the O^+ and Mg^+ zones by different symbols for different starburst ages. As expected, these temperatures are very similar. The dispersion of the data at high temperatures $T_e(\text{O II}) \geq 15000\text{K}$ is mainly due to the different starburst ages. However, at lower temperatures, which is the case for our galaxies, the dispersion is small and there is no evident separation between models with different starburst ages. We fit the relation for models with all ages by an expression

$$t_e(\text{Mg II}) = 0.4560t_e(\text{O II})^3 - 1.4262t_e(\text{O II})^2 + 2.3378t_e(\text{O II}) - 0.3675, \quad (2)$$

which is shown in Fig. 4a by solid line. We will use this fit in our subsequent analysis. However, we note that the fit in Eq. 2 is only applicable to the range $T_e(\text{O II}) \sim 9000 - 17000\text{K}$.

The Mg^+ abundance is derived from the equation

$$\frac{\text{Mg}^+}{\text{H}^+} = 2.63 \times 10^{-8} t_e(\text{Mg II})^{-0.482} 10^{2.186/t_e(\text{Mg II})} \times \frac{I(\text{Mg II } \lambda 2797 + \lambda 2803)}{I(\text{H}\beta)}, \quad (3)$$

where we use collisional strengths for the Mg II $\lambda 2797$ and $\lambda 2803$ transitions from Mendoza (1983). These collisional strengths are in very good agreement with those obtained more recently by Sigut & Pradhan (1995).

The total Mg abundance is obtained from the relation

$$\frac{\text{Mg}}{\text{H}} = ICF(\text{Mg}^+) \frac{\text{Mg}^+}{\text{H}^+}, \quad (4)$$

where the ionisation correction factor $ICF(\text{Mg}^+)$ takes all unseen stages of magnesium ionisation inside the H II region into account. To derive $ICF(\text{Mg}^+)$ we use our grid CLOUDY models and define it as the ratio $x(\text{H}^+)/x(\text{Mg}^+)$, where $x(\text{H}^+) = \text{H}^+/\text{H}$ and $x(\text{Mg}^+) = \text{Mg}^+/\text{Mg}$ are volume-averaged fractions of H^+ and Mg^+ , respectively.

In Fig. 4b we show the dependence of $ICF(\text{Mg}^+)$ on the excitation parameter O^{2+}/O . Ionisation potentials of Mg of the three ionisation stages Mg, Mg^+ , and Mg^{++} are 7.6, 15.0 and 80.1 eV, respectively. Therefore, most of magnesium in a photoionised region is in the Mg^+ and Mg^{++} stages. However, because Mg^+ is not the dominant ionic species for most nebulae and because Mg^{++} is not observed in the visible range, a rather large $ICF(\text{Mg}^+)$ is needed. Models with different starburst ages in Fig. 4b are shown by different symbols. There is a clear offset between the models with younger and older starburst ages, indicating differences in the spectral energy distribution of the ionising radiation. The fit to the data with all ages defined by equation

$$ICF(\text{Mg}^+) = \sum_{i=1}^4 a_i t_e^{b_i} \exp\left(\frac{c_i}{t_e}\right), \quad (5)$$

where coefficients a_i , b_i , and c_i are given in Table 4. The fit is produced for a wide range of $x = 0.2 - 1.0$ where ICF increases from ~ 3 to more than 100. However, the range of x in the sample galaxies (horizontal line) is smaller, corresponding to ICF s in the range $\sim 3.5 - \sim 20$ with an average value of ~ 6 . The fit closely follows the models with starburst age of 3.5 Myr corresponding to the equivalent width $\text{EW}(\text{H}\beta) \sim 100\text{\AA}$ that is typical for our galaxies.

4. Results and discussion

In Figs. 5a and 5b the dependences of $[\text{Mg}/\text{O}] = \log(\text{Mg}/\text{O}) - \log(\text{Mg}/\text{O})_{\odot}$ on $12+\log\text{O}/\text{H}$ are shown for the 45 spectra where the Mg II emission lines was detected. We note also that in many cases blue-shifted Mg II absorption near the Mg II $\lambda 2797\text{\AA}$ emission line is present which may indicate of stellar winds from cool massive stars, such as LBVs (see, for instance, J0207+0047, J0925+2709, J1045+3225 in Fig. 2). The encircled galaxies are those with no clear presence of blue-shifted absorption profiles (Fig. 5a). There is no obvious offset of the encircled points as compared to other data. This testifies to the correctness of Mg II $\lambda 2797$ and $\lambda 2803$ line measurements in

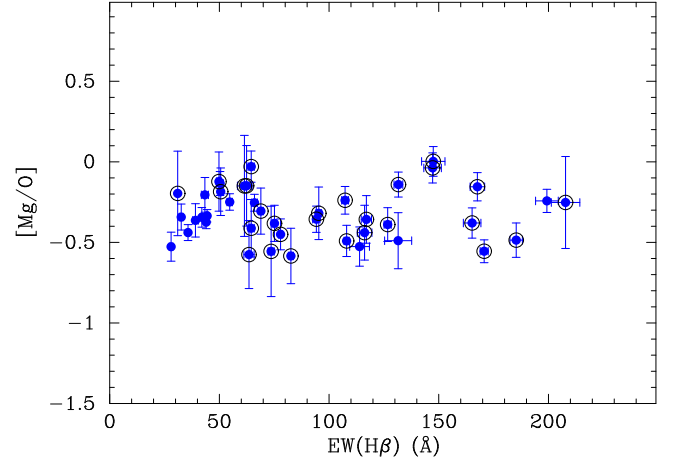


Fig. 6. Dependence of the magnesium-to-oxygen abundance ratio relative to the solar value $[\text{Mg}/\text{O}]$ on the equivalent width $\text{EW}(\text{H}\beta)$ of the $\text{H}\beta$ emission line. The galaxies with the measured $[\text{O III}]\lambda 4363\text{\AA}$ line are encircled.

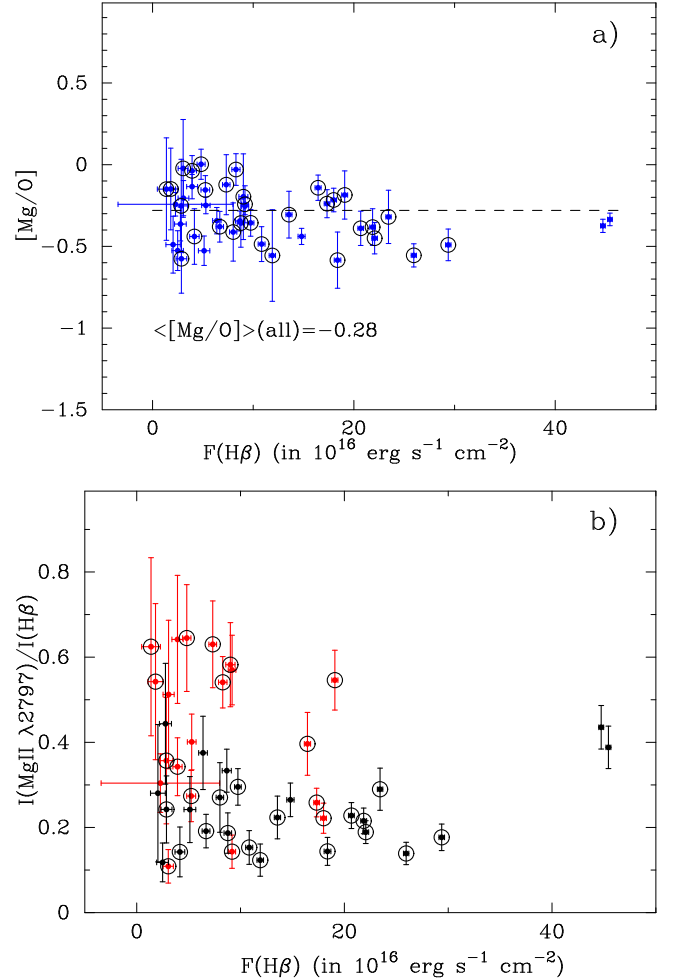


Fig. 7. Dependence of the magnesium-to-oxygen abundance ratio relative to the solar value $[\text{Mg}/\text{O}]$ (a) and the $I(\text{Mg II } \lambda 2797)/I(\text{H}\beta)$ ratio (b) on observed fluxes of the $\text{H}\beta$ emission line corrected for both the Milky Way and internal extinctions. (a) All sample galaxies are shown. (b) The same as in (a) but H II regions with $[\text{Mg}/\text{O}] \geq -0.3$ being shown in red and those with $[\text{Mg}/\text{O}] < -0.3$ in black. The galaxies with measured $[\text{O III}]\lambda 4363\text{\AA}$ line are encircled.

Table 6. Magnesium abundances collected from the literature

(1)	N (item) (2)	[X/Y] ^a (3)	Value (4)	reference (5)	Comments (6)
	1	[Mg/H] ^c	-1.22	1	Cold Galactic clouds
	2	[Mg/H] ^c	-0.62	1	Warm Galactic clouds
	3	[Mg/O]	-1.00	1	Cold Galactic clouds
	4	[Mg/O]	-0.40	1	Warm Galactic clouds
	5	[Mg/H] ^c	-0.37	1	Weaker low-velocity (WLV) absorption of interstellar clouds toward 23 Ori (<i>HST</i>)
	6	[Mg/H] ^c	-0.74	1	Strong low-velocity (SLV) absorption in H II gas toward 23 Ori (<i>HST</i>)
	7	[Mg/S]	-0.51	1	WLV absorption of interstellar clouds toward 23 Ori (<i>HST</i>)
	8	[Mg/S]	-0.89	1	SLV absorption in H II gas toward 23 Ori (<i>HST</i>)
	9	[Mg/H] ^c	-0.46	2	Mean value of ISM toward 70 early type stars (<i>Copernicus</i>)
LISM ^b	10	[Mg/H] ^c	-0.24	3	Interstellar cloud <i>A</i> in the direction of ζ Oph
	11	[Mg/H]	-0.90	3	Interstellar cloud <i>B</i> in the direction of ζ Oph
	12	[Mg/O]	-0.48	3	ISM, <i>A</i> component in the direction of ζ Oph
	13	[Mg/O]	-0.69	3	ISM, <i>B</i> component in the direction of ζ Oph
	14	[Mg/O]	-1.21	4	α CMa A, 1st component of LISM within 100 pc (<i>HST</i>)
	15	[Mg/O]	-0.61	4	α CMa A, 2nd component of LISM within 100 pc (<i>HST</i>)
	16	[Mg/O]	-0.89	4	G191-B2B 1st component of LISM within 100 pc (<i>HST</i>)
	17	[Mg/O]	+0.28	4	G191-B2B 2nd component of LISM within 100 pc (<i>HST</i>)
	18	[Mg/O]	-0.46	4	Weighted mean of LISM within 100 pc (<i>HST</i>)
	19	[Mg/H] ^c	-0.9	5	ζ Pyx (observations of ISM toward 8 cool (G4-K0) giants, <i>IUE</i>)
	20	[Mg/H] ^c	-0.9	5	HD 81101 (<i>IUE</i>)
	21	[Mg/H] ^c	-0.8	5	ζ Vol, 1st component (<i>IUE</i>)
	22	[Mg/H] ^c	-0.9	5	ζ Vol, 2nd component (<i>IUE</i>)
	23	[Mg/H] ^c	+0.023	6	averaged values for 25 planetary nabulae (PNe), Mg II $\lambda 4481$
PNe ^d	24	[Mg/H] ^c	0.0	7	planetary nebula IC 418, (<i>IUE</i>), Mg II $\lambda\lambda 2797, 2803$
	25	[Mg/H] ^c	-1.1	7	planetary nebula NGC 2440, (<i>IUE</i>), Mg II $\lambda\lambda 2797, 2803$
	26	[Mg/H] ^c	-0.64	7	planetary nebula IC 4997, (<i>IUE</i>), Mg II $\lambda\lambda 2797, 2803$
	27	[Mg/O] ^e	-0.94	8	Mg II $\lambda 4481$ line, based on observation of Orion by Esteban et al. (2004)
H II regions	28	[Mg/O]	-1.00	8	Mg II $\lambda 4481$ line, based on observation of Orion by Esteban et al. (2004)
	29	[Mg/O]	-0.35	8	30 Dor, based on Mg II $\lambda 4481$ and Mg I $\lambda\lambda 4561, 4571$
	30	[Mg/O] ^f	-0.67	8	30 Dor, based on Mg II $\lambda 4481$ and Mg I $\lambda\lambda 4561, 4571$
	31	[Mg/S] ^g	-0.09	9	gas-phase abundances obtained in absorption system along the GRB HG 050820
	32	[Mg/S]	-0.18	9	absorption system toward the GRB HG 050820
	33	[Mg/S]	0.0	10	absorption system toward the Q 0100+13 ($z_{abs}=2.309$)
QSO- -DLA- -GRB	34	[Mg/S]	-0.04	11	absorption system toward the Q B0841+129 ($z_{DLA}=2.375$)
	35	[Mg/S]	+0.03	11	absorption system toward the Q B0841+129 ($z_{DLA}=2.476$)
	36	[Mg/S]	-0.07	12	absorption system toward the Q 1101-264 ($z_{abs}=1.838$)
	37	[Mg/S]	-0.04	13	mean value for absorption system toward the Q 1331+17 ($z_{abs}=1.776$)
	38	[Mg/S]	+0.13	14	data for ~ 85 DLA systems (Keck spectra) FJ 0812+32 ($z_{abs}=2.6263$)
	39	[Mg/S]	-0.49	14	data for ~ 85 DLA systems (Keck spectra) J 0900+42 ($z_{abs}=3.2458$)

References. [1] Welty et al. (1999), [2] Murray (1983), [3] Savage et al. (1992), [4] Redfield & Linsky (2004), [5] Molaro et al. (1986), [6] Dinerstein et al. (2012), [7] Middlemass (1988), [8] Peimbert & Peimbert (2010), [9] Prochaska et al. (2007a), [10] Dessauges-Zavadsky et al. (2004), [11] Dessauges-Zavadsky et al. (2007), [12] Dessauges-Zavadsky et al. (2003), [13] Dessauges-Zavadsky et al. (2006), [14] Prochaska et al. (2007)

^aAll data were recalculated with solar abundances by Asplund et al. (2009).

^bLocal Interstellar Medium.

^cThe solar abundance pattern is adopted for the local interstellar medium.

^dPlanetary nebulae.

^eAdopted solar vicinity ISM abundances, average from B stars and solar neighbourhood abundances corrected for Galactic chemical evolution since the Sun was formed (Peimbert & Peimbert 2010).

^fAdopted abundances by Tsamis & Péquignot (2005).

^gSolar abundances by Asplund et al. (2005) are assumed, following Prochaska et al. (2007a).

cases when the continuum is placed at the bottom of absorption profiles. In Fig. 5b we divide the sample between objects with bright Mg II lines ($I(\lambda 2797\text{\AA})/I(H\beta) \geq 0.3$) and weak Mg II lines ($I(\lambda 2797\text{\AA})/I(H\beta) < 0.3$). Encircled galaxies in (b) are those where [O III] $\lambda 4363\text{\AA}$ emission is detected. A slight shift of H II regions with bright Mg II emission line $\lambda 2797$ to lower metallicity is seen in Fig. 5b.

Table 5 summarises spectroscopic parameters for all 65 spectra, where we show the galaxy name, the oxygen abundance $12+\log O/H$, the quantity [Mg/O], and the equivalent width EW(H β) of the H β emission line in \AA . We adopt $\log(Mg/O)_{\odot} = -1.09$ (Asplund et al. 2009). We note that both O and Mg are subject to depletion onto dust. However, oxygen is by a factor

of ~ 10 more abundant than magnesium. Therefore, the quantity $[\text{Mg}/\text{O}]$ is mainly a characteristic of the magnesium depletion.

The dependences of $[\text{Mg}/\text{O}]$ on $\text{EW}(\text{H}\beta)$ are shown in Fig. 6. Three H II regions from our sample have $\text{EW}(\text{H}\beta) > 250\text{\AA}$ and are outside of the figure. Their $[\text{Mg}/\text{O}]$ values range between -0.02 and -0.24 (see Table 5), similar to the range of $[\text{Mg}/\text{O}]$ for the entire sample. The galaxies with measured $[\text{O III}]\lambda 4363\text{\AA}$ emission line are encircled. There is no trend in $[\text{Mg}/\text{O}]$ with $\text{EW}(\text{H}\beta)$ in Fig. 6. The $\text{EW}(\text{H}\beta)$ is a characteristic of the starburst age, hence of the excitation parameter x . Therefore, the absence of any correlation in Fig. 6 indicates the correctness of the correction for unseen stages of Mg ionisation.

To additionally check the accuracy of our measurements and our magnesium and oxygen abundance determinations, we show in Fig. 7 the dependence of the magnesium-to-oxygen abundance ratio relative to solar value $[\text{Mg}/\text{O}]$ (Fig. 7a) and $I(\text{Mg II } \lambda 2797)/I(\text{H}\beta)$ (Fig. 7b) on the observed fluxes of $\text{H}\beta$ emission lines corrected for both the Milky Way and internal extinctions for all sample galaxies. The galaxies with measured $[\text{O III}]\lambda 4363\text{\AA}$ emission line are encircled. No differences in the distributions of the galaxies with measured $[\text{O III}]\lambda 4363\text{\AA}$ line and without this line is found in Figs. 5b, 6, and 7a,b. Thus, in the following discussion we use all the data together obtained with the direct and semi-empirical methods. There is also no clear trend in $[\text{Mg}/\text{O}]$ and $I(\text{Mg II } \lambda 2797)/I(\text{H}\beta)$ with corrected fluxes of $\text{H}\beta$. This is also evidence for the accuracy of our determinations.

We do not find any obvious trend in $[\text{Mg}/\text{O}]$ with oxygen abundance in the entire range of $12 + \log \text{O}/\text{H} = 7.52 - 8.44$ (Fig. 5). The mean value of the Mg/O ratio is by a factor of ~ 2 lower than the solar value, implying moderate Mg depletion of $\sim 50\%$ in the dust phase. This depletion is significantly higher than the mean value obtained by Dinerstein et al. (2012) for PNe. They derived Mg/O close to the solar value using the recombination Mg II $\lambda 4481$ emission line. These differences can be explained by the known discrepancy between values derived from recombination lines (RL) and collisionally excited lines (CEL) (Esteban et al. 2009; Peimbert et al. 2005; Davey et al. 2000; Guseva et al. 2011). Abundances obtained from RLs tend to be higher than those derived from CEL lines. The origin of the nebular abundance discrepancy problem is currently not known. On the other hand, Barlow et al. (2003) and Wang & Liu (2007) do not empirically find any such discrepancy for Mg/H. Moreover, the Mg fraction in dust also obtained using the recombination Mg II $\lambda 4481$ emission line is much higher in 30 Doradus (72%) and in the Orion nebula (91%) (Peimbert & Peimbert 2010) than in the PNe analysed by Dinerstein et al. (2012).

The negative values of $[\text{Mg}/\text{O}]$ in our galaxies can be due to the absorption of the Mg II $\lambda 2797$, $\lambda 2803$ emission by the interstellar gas outside the H II regions. The spectral resolution of the SDSS spectra is insufficient to separate the Mg II absorption and emission to estimate the effect of the interstellar absorption and to correct emission-line intensities for this effect. An additional source of uncertainties may arise due to the presence of broad blue-shifted absorption lines in many spectra of our sample superposed with the emission lines (Fig. 2). One of the most evident cases is the galaxy J1045+3225. These lines are likely to be broad lines with P Cygni profiles produced by cool massive stars (red supergiants, LBVs) with a stellar wind (e.g. Hillier et al. 2001). The presence of these lines will introduce uncertainties into the placement of the continuum for measurements of the intensities of nebular emission lines. We measure magnesium emission lines placing the continuum at the bottom of the ab-

sorption lines when it is obviously seen in the observed spectra as described above. In spectra of some other galaxies there is no clear evidence of the blue-shifted broad absorption (see Fig. 2). To verify the effect of this absorption on the derived Mg abundance, we divided the objects in Fig. 5a into two samples, those with and those without evident blue-shifted broad absorption. It is very important that the encircled galaxies without blue-shifted absorption have the same $[\text{Mg}/\text{O}]$ and dispersion as other galaxies.

Summarising, we find that the Mg depletion in our galaxies is probably present but at a relatively low level with roughly half of the Mg in dust. This level of Mg depletion onto dust can be considered as an upper limit because the interstellar absorption is not known and is difficult to be taken into account. For comparison, Jenkins (2009) found the relative proportions of different elements that are incorporated into dust at different stages of grain growth based on gas-phase element abundances for 17 different elements over 243 sight lines in the local part of our Galaxy. According to them $\sim 70\%$ ($\sim 50\%$ on Fig. 5 by Jenkins 2009) of magnesium is locked onto dust grains and $\sim 95\%$ ($\sim 90\%$ on Fig. 7 by Jenkins 2009) of iron is also in solid form (see also Fig. 1 by Jenkins 2009).

4.1. Comparison of magnesium depletion in objects of different types

We compared magnesium depletion obtained for our low-metallicity, emission-line star-forming galaxies with available data from the literature for objects of different types. There are many DLA and QSO absorption systems with magnesium abundance determination from Mg II $\lambda 2797$, $\lambda 2803$ lines. However, only an upper limit to the MgII abundance has been obtained in the majority of the cases. We include in Table 6 only those objects for which the exact values of number densities for hydrogen, magnesium, and oxygen (or sulphur) have been collected. We recalculated all data with solar abundances by Asplund et al. (2009) where it was necessary. To be more specific, we display in Fig. 8a all data from Table 6, indicating the different type of objects by different colours and symbols. The value of $[\alpha/\text{H}]$ is in terms of $[\text{S}/\text{H}]$ for DLA-QSA-GRB absorption systems and $[\text{O}/\text{H}]$ for LISM, H II regions, and our sample galaxies.

Following Leboutteiller et al. (2008) we adopted the oxygen abundance of 30 Dor in the LMC to be a factor of ~ 0.6 lower than the solar value. The mean oxygen abundance of our Mg sample is $12 + \log \text{O}/\text{H} = 8.02$ for 45 H II regions. A solar abundance of $12 + \log \text{O}/\text{H} = 8.69$ (Asplund et al. 2009) was adopted for the local interstellar medium (clouds toward Galactic stars and PNe). Following Peimbert & Peimbert (2010) an oxygen abundance of $12 + \log \text{O}/\text{H} = 8.65$ was adopted for the Orion nebula (determination based on the observations by Esteban et al. 2004). In all comparisons for DLA absorption systems we used the non-refractory element sulphur for metallicity estimation and for the determination of magnesium depletion because oxygen absorption lines are generally saturated (e.g. Prochaska et al. 2007).

In Fig. 8b we compare $[\text{Mg}/\text{O}]$ and $[\alpha/\text{H}]$ averaged for each of four types of objects (LISM, H II regions, our sample, and DLA-QSO-GRB absorption systems). The averaged values of $[\text{Mg}/\text{O}]$ and $[\alpha/\text{H}]$ are obtained from the logarithms of the average $\langle \text{Mg}/\text{O} \rangle$ and $\langle \alpha/\text{H} \rangle$.

This is to be compared to iron depletion. Rodríguez & Rubin (2005) discovered the trend of increasing Fe depletion at higher oxygen abundance. For the Galactic H II regions and PNe they obtained high Fe depletion, with

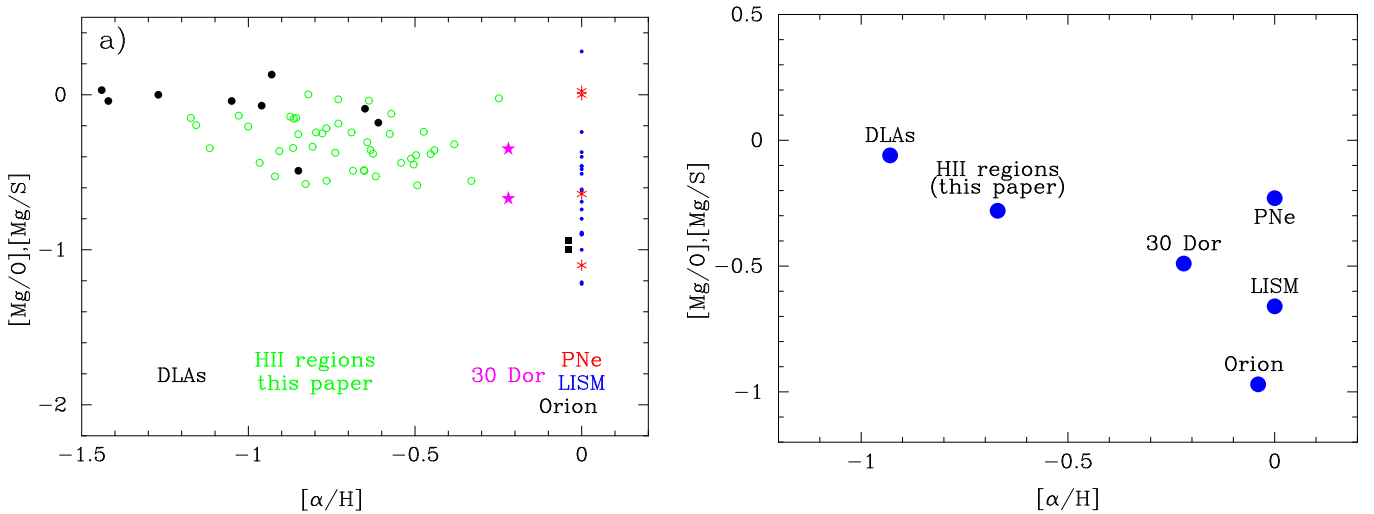


Fig. 8. (a) Comparison of magnesium depletion for data available from the literature (denoted by different colours and symbols) and (b) comparison of the magnesium depletion averaged for objects of each of four types (LISM (Local interstellar medium), H II regions, our Mg II sample (this paper), and DLA-QSO-GRB (Damped Ly α absorption – Quasi-stellar object – Gamma-ray burst) absorption systems. $[\alpha/\text{H}]$ is $[\text{O}/\text{H}]$ for LISM, H II regions, and our sample galaxies, and $[\text{S}/\text{H}]$ for DLA-QSA-GRB absorption systems.

fewer than 5% of their Fe atoms in the gas phase, whereas the metal-deficient blue compact galaxy SBS 0335–052 could have only from 13% to 40% of Fe in the gas phase. Izotov et al. (2006) also obtained the trend in Fe depletion with metallicity. Considering the iron depletion in low-metallicity, star-forming emission-line galaxies they find that $\sim 80\%$ of iron is confined in dust in galaxies with $12+\log\text{O}/\text{H} \sim 8.0$ (their Fig. 111).

Despite a wide spread of points for the individual objects (Fig. 8a), there is also a clear trend in averaged $[\text{Mg}/\text{O}]$ with metallicity in Fig. 8b for different types of objects, indicating that the depletion is higher for higher metallicity objects. Thus, we confirm the previous findings by Jenkins (2009) of increasing Mg depletion with increasing metallicity.

5. Conclusions

We have presented 65 SDSS spectra of low-metallicity, emission-line star-forming galaxies with redshifts $z \sim 0.36 - 0.70$, with the aim of studying the interstellar magnesium abundance as derived from the resonance emission-line doublet Mg II $\lambda 2797$, $\lambda 2803$. This emission is detected in 45 galaxies, or in more than two thirds of the sample. Our main results are as follows:

1. Using the grid of 576 CLOUDY photoionised H II region models, we obtained fits of the electron temperature $T_e(\text{Mg II})$ in the Mg^+ zone as a function of the electron temperature $T_e(\text{O II})$ in the O^+ zone. Furthermore, using the same CLOUDY models we obtained fits of the ionisation correction factor $ICF(\text{Mg}^+)$ as a function of the excitation parameter $x = \text{O}^{2+}/\text{O}$.

2. We derived oxygen and magnesium abundances. The $[\text{O III}] \lambda 4363$ emission line is seen in $\sim 63\%$ of the sources of the total sample and $\sim 70\%$ of the galaxies in which the Mg II lines were detected, allowing an accurate abundance determination with the direct T_e method. The element abundances in the remaining galaxies we are derived using a semi-empirical method that is based on strong nebular oxygen lines. Data obtained with the two methods are indistinguishable in all distributions. The oxygen abundances $12+\log\text{O}/\text{H}$ for the sample galaxies are in the relatively wide range from 7.52 to 8.44.

3. We found that the Mg/O abundance ratio in our galaxies is lower by a factor of two than in the Sun, implying a moderate Mg depletion onto dust with $\sim 50\%$ of magnesium confined in dust. This level of depletion is higher than in high-redshift, low-metallicity damped Ly α (DLA) systems with measured Mg abundances. However, it is much lower than in H II regions with higher metallicity (e.g., in the Orion nebula and 30 Doradus, where the fraction of Mg in dust is 91% and 72%, respectively), in PNe (averaged value) and in interstellar clouds of the LISM.

4. Despite a wide spread of points for the individual determinations there is a clear trend in $[\text{Mg}/\text{O}]$ or $[\text{Mg}/\text{S}]$ with metallicity when averaged magnesium abundance and metallicity for different types of objects is used. This implies that the magnesium depletion is higher in higher metallicity objects.

Acknowledgements. N.G.G. and Y.I.I. acknowledge the hospitality of the Max-Planck Institute for Radioastronomy, Bonn, Germany. This research made use of the NASA/IPAC Extragalactic Database (NED), which is operated by the Jet Propulsion Laboratory, California Institute of Technology, under contract with the National Aeronautics and Space Administration. Funding for the Sloan Digital Sky Survey (SDSS), and SDSS-II has been provided by the Alfred P. Sloan Foundation, the Participating Institutions, the National Science Foundation, the U.S. Department of Energy, the National Aeronautics and Space Administration, the Japanese Monbukagakusho, and the Max Planck Society, and the Higher Education Funding Council for England.

References

- Aller, L. H. 1984, *Physics of Thermal Gaseous Nebulae* (Dordrecht: Reidel)
- Asplund, M., Grevesse, N., & Sauval, A. J. 2005, *ASP Conference Series*, 336, 25
- Asplund, M., Grevesse, N., Sauval, A. J., & Scott, P. 2009, *ARAA*, 47, 481
- Barlow, M. J., Liu, X.-W., Péquignot, D., Storey, P. J., Tsamis, Y. G., & Morisset, C. 2003, in *Planetary nebulae: their evolution and role in the Universe*, IAU Symposium, 209, 373
- Bordoloi, R., et al. 2011, *ApJ*, 743, 10
- Bouché, N., Murphy, M. T., Péroux, C., Csabai, I. & Wild, V. 2006, *MNRAS*, 371, 495
- Bruzual, G., & Charlot, S. 2003, *MNRAS*, 344, 1000
- Cardelli, J. A., Clayton, G. C., & Mathis, J. S. 1989, *ApJ*, 345, 245
- Davey, A. R., Storey, P. J., & Kisielius, R. 2000, *A&AS*, 142, 85
- Dessauges-Zavadsky, M., Péroux, C., Kim, T.-S., D’Odorico, S., & McMahon, R. G. 2003, *MNRAS*, 345, 447
- Dessauges-Zavadsky, M., Calura, F., Prochaska, J. X. D’Odorico, S., & Matteucci, F. 2004, *A&A*, 416, 79

- Dessauges-Zavadsky, M., Prochaska, J. X., D'Odorico, S., Calura, F., & Matteucci, F. 2006, *A&A*, 445, 93
- Dessauges-Zavadsky, M., Calura, F., Prochaska, J. X., D'Odorico, S., & Matteucci, F. 2007, *A&A*, 470, 431
- Dinerstein, H. L., Prasla, F., & Speck, A. K. 2012, *American Astronomical Society, AAS Meeting No 219*, No 343.01
- Esteban, C., Bresolin, F., Peimbert, M., et al. 2009, *ApJ*, 700, 654
- Esteban, C., Peimbert, M., García-Rojas, J., Ruiz, M. T., Peimbert, A., & Rodríguez, M. 2004, *MNRAS*, 355, 229
- Ferland, G. J., Korista, K. T., Verner, D. A., Ferguson, J. W., Kingdon, J. B., & Verner, E. M. 1998, *PASP*, 110, 761
- Grevesse, N., & Sauval, A. J. 1998, *Space Science Reviews*, 85, 161
- Guseva, N. G., Izotov, Y. I., Stasińska, G., Fricke, K. J., Henkel, C., & Papaderos, P. 2011, *A&A*, 529, 149
- Hillier, D. J., & Miller, D. L. 1998, *ApJ*, 496, 407
- Hillier, D. J., Davidson, K., Ishibashi, K., & Gull, T. 2001, *ApJ*, 553, 837
- Izotov, Y. I., & Thuan, T. X. 2007, *ApJ*, 665, 1115
- Izotov, Y. I., Thuan, T. X., & Lipovetsky, V. A. 1994, *ApJ*, 435, 647
- Izotov, Y. I., Thuan, T. X., & Lipovetsky, V. A. 1997, *ApJS*, 108, 1
- Izotov, Y. I., Stasińska, G., Meynet, G., Guseva, N. G., & Thuan, T. X. 2006, *A&A*, 448, 955
- Jenkins, E. B. 2009, *ApJ*, 700, 1299
- Lebouteiller, V., Bernard-Salas, J., Brandl, B., et al. 2008, *ApJ*, 680, 398
- Leitherer, C., Schaerer, D., Goldader, J. D., Gonzalez Delgado, R. M., Robert, C., Kune D. F., de Mello, D. F., Devost, D., & Heckman, T. M. 1999, *ApJS*, 123, 3
- Lilly, S. J., et al. 2007, *ApJS*, 172, 70
- Lundgren, B. F., Brunner, R. J., Donald G. York, D. G., et al. 2009, *ApJ*, 698, 819
- Mendoza, C. 1983, in *Planetary Nebulae*, ed. D. R. Flower, Dordrecht, D. Reidel Publishing Co., p.143
- Meynet, G., Maeder, A., Schaller, G., Schaerer, & D. Charbonnel, C. 1994, *A&AS*, 103, 97
- Middlemass, D. 1988, *MNRAS*, 231, 1025
- Molaro, P., Vladilo, G., & Beckman, J. E. 1986, *AJ*, 161, 339
- Murray, M. J. 1983, *Irish Astronomical Journal*, 16, 41
- Nestor, D. B., Turnshek, D. A., & Rao, S. M. 2005, *ApJ*, 628, 637
- Oegerle, W. R., Kondo, Y., Stencel, R. E., & Weiler, E. J. 1982, *ApJ*, 252, 302
- Pauldrach, A. W. A., Hoffman, T. L., & Lennon, M. 2001, *A&A*, 375, 161
- Peimbert, A., Peimbert, M., & Ruiz, M. T. 2005, *ApJ*, 634, 1056
- Peimbert, A., & Peimbert, M. 2010, *ApJ*, 724, 791
- Péquignot, D., & Stasińska, G. 1980, *A&A*, 81, 121
- Perinotto, M., & Patriarchi, P. 1980, *ApJ*, 235, L13
- Prochaska, J. X., Chen, H.-W., Bloom, J. S., et al. 2007, *ApJS*, 168, 231
- Prochaska, J. X., Wolfe, A. M., Howk, J. C., Gawiser, E., Burles, S. M., & Cooke, J. 2007, *ApJS*, 171, 29
- Prochter, G. E., Prochaska, J. X., & Burles, S. M. 2006, *ApJ*, 639, 766
- Quider, A. M., Nestor, D. B., Turnshek, D. A., et al. 2011, *AJ*, 141, 137
- Redfield, S., & Linsky, J. L. 2004, *ApJ*, 602, 776
- Rodríguez, M., & Rubin, R. H. 2005, *ApJ*, 626, 900
- Sargent, W. L. W., Steidel, C. C., & Boksenberg, A. 1988, *ApJ*, 334, 22
- Savage, B. G., Cardelli, J. A., & Sofia, U. J. 1992, *ApJ*, 401, 706
- Sigut, T. A. A., & Pradhan, A. K. 1995, *J.Phys.B: At.Mol.Opt.Phys.* 28, 4879
- Snow, T. P., & Witt, A. N. 1996, *ApJ*, 468, L65
- Stasińska, G., & Izotov, Y. I. 2003, *A&A*, 397, 71
- Steidel, C. C., & Sargent, W. L. W. 1992, *ApJS*, 80, 1
- Thuan, T. X., Izotov, Y. I., & Lipovetsky, V. A. 1995, *ApJ*, 445, 108
- Tsamis, Y. G., & Péquignot, D. 2005, *MNRAS*, 364, 687
- Wang, W., & Liu, X.-W. 2007, *MNRAS*, 381, 669
- Welty, D. E., Hobbs, L. M., Lauroesch, J. T., et al. 1999, *ApJS*, 124, 465
- York, D. G., Adelman, J., Anderson, J. E., et al. 2000, *AJ*, 120, 1579
- York, D. G., Khare, P., Vanden Berk, D., et al. 2006, *MNRAS*, 367, 945
- Zhu, G., & Ménard, B. 2012, *ApJ*, in press, preprint arXiv:astro-ph1211.6215v1

Table 2. —*Continued.*

Ion	$I(\lambda)/I(H\beta)$	$I(\lambda)/I(H\beta)$	$I(\lambda)/I(H\beta)$	$I(\lambda)/I(H\beta)$	$I(\lambda)/I(H\beta)$	$I(\lambda)/I(H\beta)$	$I(\lambda)/I(H\beta)$
GALAXY							
2804 Mg II	...	0.25±0.09					
3727 [O II]	2.27±0.09	2.94±0.12					
3868 [Ne III]	0.36±0.03	0.41±0.04					
4101 H δ	0.29±0.03	0.29±0.04					
4340 H γ	0.47±0.03	0.47±0.03					
4363 [O III]	0.05±0.01	0.04±0.02					
4861 H β	1.00±0.03	1.00±0.04					
4959 [O III]	1.32±0.03	1.34±0.04					
5007 [O III]	4.06±0.09	3.97±0.10					
$C(H\beta)$ (MW)	0.05	0.05					
$C(H\beta)$ (int)	0.47	0.50					
EW _{abs}	0.00	2.09					
EW(H β)	100.90	64.51					
$F(H\beta)^a$	16.88	8.01					

^aUncorrected H β flux in 10^{-16} erg s $^{-1}$ cm $^{-2}$